Molecular BioSystems

RSC Publishing

PAPER

Solution conformational features and interfacial properties of an intrinsically disordered peptide coupled to alkyl chains: a new class of peptide amphiphiles†‡

Cite this: *Mol. BioSyst.*, 2013, **9**, 1401

Antonella Accardo,[ab] Marilisa Leone,[b] Diego Tesauro,[ab] Rosa Aufiero,[c] Anaïs Bénarouche,[c] Jean-François Cavalier,[c] Sonia Longhi,[d] Frederic Carriere[c] and Filomena Rossi*[ab]

Received 8th November 2012,
Accepted 14th February 2013

DOI: 10.1039/c3mb25507g

www.rsc.org/molecularbiosystems

Owing to the large panel of biological functions of peptides and their high specificity and potency, the development of peptide-based therapeutic and diagnostic tools has received increasing interest. Peptide amphiphiles (PAs) are an emerging class of molecules in which a bioactive peptide is covalently conjugated to a hydrophobic moiety. Due to the coexistence in the molecule of a hydrophilic peptide sequence and a hydrophobic group, PAs are able to self-assemble spontaneously into a variety of nanostructures, such as monolayers, bilayers, and vesicles. In this work we have synthesized a disordered peptide, henceforth called R11, and two lipophilic derivatives of R11 bearing two alkyl chains, connected or not to R11 by an ethoxylic-based linker. The structural properties in solution of these new PAs were investigated using CD and NMR. R11 lipophilic derivatives display typical features of PAs, such as the formation of micelles and unilamellar vesicles. In addition, their surface properties were studied using Langmuir monomolecular films and the results obtained support the formation of molecular aggregates upon compression of the PA films. The presence of the alkyl chains induces not only the self-assembly of these new PAs into supramolecular aggregates but also a gain of structure within the disordered peptide.

1. Introduction

Peptides are the main class of biological macromolecules able to regulate physiological processes by acting as growth factors, antibiotics, neurotransmitters, and hormones.[1–5] Owing to the large array of biological functions of peptides and their high specificity and potency, the development of peptide-based therapeutic and diagnostic tools has received increasing interest. In this contest, it is customary to replace the definite peptidic region using organic scaffolds with the aim of developing novel molecular entities that would act as pharmacological chaperones.[6,7] Numerous endogenous peptides are natively disordered, *i.e.* they exhibit a random coil structure in solution. It is also well known that under different physiological conditions and biochemical environments, a number of biological intrinsically disordered peptides misfold and aggregate into well-defined amyloid fibrils, including the β-amyloid (Aβ) peptide associated with Alzheimer's diseases and the islet amyloid polypeptide (IAPP) related to type 2 diabetes.[8–11] Intrinsically disordered proteins (IDPs) have recently gathered much interest because of their role in biological processes such as molecular recognition and their ability to undergo stimulus-responsive conformational changes.[12,13] Overall, the flexibility of the conformational ensemble of natively disordered proteins and/or peptides prompts the formation of transient complexes with binding partners characterized by a low affinity because of the entropic cost associated with the disorder-to-order transition upon binding. Interactions with binding partners ultimately regulate the balance between folding, misfolding and fibrillogenesis,

[a] *Dipartimento di Farmacia and CIRPeB, Università degli Studi Federico II di Napoli, Via Mezzocannone, 16 80134 Naples, Italy. E-mail: filomena.rossi@unina.it; Fax: +39 0812534574; Tel: +39 0812536682*
[b] *Istituto di Biostrutture e Bioimmagini (IBB) CNR, Via Mezzocannone, 16 80134 Naples, Italy*
[c] *CNRS, Aix-Marseille Université, Enzymologie Interfaciale et Physiologie de la Lipolyse UMR 7282, Marseille, France*
[d] *Architecture et Fonction des Macromolécules Biologiques, UMR 7257, CNRS and Aix-Marseille Université, Marseille, France*

† Dedicated to prof. Ettore Benedetti on the occasion of his 72nd birthday.

‡ Electronic supplementary information (ESI) available. See DOI: 10.1039/c3mb25507g

thereby modulating the biological activities and proteotoxicities of polypeptides.[14] The possibility to control the transition between different structural states offers an opening for employment of IDPs in molecular recognition, biosensor applications, improvement of therapeutics, and in bionanotechnologies.[15,16] A possible route to achieve this goal consists in anchoring the peptide at supramolecular aggregates by covalent approaches. Peptide amphiphiles (PAs) are an emerging class of molecules in which a bioactive peptide is covalently conjugated to a hydrophobic moiety, commonly one or two alkyl tails. Supramolecular structures obtained by self-assembling of PA molecules are characterized by typical features with respect to traditional surfactant molecules. Due to the coexistence in the molecule of a hydrophilic peptide sequence and a hydrophobic tail, they are able to self-assemble spontaneously into a variety of nanostructures, such as monolayers, bilayers, vesicles, elongated worm- or rod-like micelles or spherical micelles.[17–22] Many other PAs form fibers and gels, composed of elongated micelles, in which bioactive sequences are perpendicular to their long axis at near van der Waals density.[23] In this spatial arrangement, the peptide moiety remains at the periphery of the nanostructure, which enables different chemical and biological functionalities including the ability to allow formation of pores in membranes,[24] or to reach in a selective way a biological target,[25] such as membrane receptors overexpressed by cancerous cells. In all cases, the peptide availability on nanostructures is not the unique requirement for receptor binding: a disordered peptide needs to be able to adopt a specific conformation to assure high affinity and selectivity in ligand–protein binding processes.[26] Moreover, an important design consideration for peptide-based constructs is the ability of the peptide to retain its function, which is often correlated with its secondary structure. Small peptide sequences isolated from parent proteins generally lose their secondary structure, which can be detrimental to their activity.[27,28] In order to extend the study of PAs, we have herein synthesized an intrinsically disordered peptide, henceforth called R11, and two lipophilic derivatives of R11 bearing two alkyl chains (Fig. 1). Using CD and NMR spectroscopy, we have investigated the structural properties of this new class of PAs. Their surface properties were investigated using Langmuir monomolecular films.

2. Materials and methods

2.1. Chemicals

Protected N^{α}-Fmoc-amino acid derivatives, Rink amide MBHA resin and coupling reagents were purchased from Calbiochem-Novabiochem (Laufelfingen, Switzerland). Fmoc-Tyr[PO(OBzl)OH]-OH was purchased from DBA Italia (Italy). Fmoc-21-amino-4,7,10,13,16,19-hexaoxaheneicosanoic acid (Fmoc-Ahoh-OH) was purchased from Neosystem (Strasbourg, France). *N*,*N*-Dioctadecylsuccinamic acid was synthesized according to published methods.[29] All other chemicals were commercially available from Sigma-Aldrich or Fluka (Buchs, Switzerland) or LabScan (Stillorgan, Dublin, Ireland) and were used as received unless otherwise stated. Preparative RP-HPLCs were carried out on a LC8 Shimadzu HPLC system (Shimadzu Corporation, Kyoto, Japan) equipped with a UV lambda-Max Model 481 detector using Phenomenex (Torrance, CA) C18 and C4 (300 Å, 250 × 21.20 mm, 5 μ) columns for R11 peptide and $(C18)_2$R11 and $(C18)_2$-L1-R11 PAs. Elution solvents are H_2O/0.1% TFA (A) and CH_3CN/0.1% TFA (B), from 20% to 95% over 20 minutes at 20 mL min^{-1} flow rate. Purity and identity were assessed by analytical LC–MS analyses by using Finnigan Surveyor MSQ single quadrupole electrospray ionization (Finnigan/Thermo Electron Corporation San Jose, CA), column: C18/C4-Phenomenex eluted with an H_2O/0.1% TFA (A) and CH_3CN/0.1% TFA (B) from 20% to 95% over 20 minutes at 1 mL min^{-1} flow rate.

2.2. Structural predictions

Predictions of secondary structure and structural disorder were performed by the MeDor metaserver of disorder,[17] freely available at http://www.vazymolo.org/MeDor/index.html.

2.3. Peptide synthesis

The R11 peptide was synthesized by using standard solid-phase 9-fluorenylmethoxycarbonyl (Fmoc) procedures. The Rink amide MBHA resin (substitution 0.65 mmol g^{-1}) was used as the solid-phase support, and synthesis was performed on a scale of 0.1 mmol. The elongation of peptide was achieved by sequential addition of Fmoc-AA-OH with PyBOP/HOBt and DIPEA (1 : 1 : 2) as coupling reagents, in DMF in pre-activation mode. All couplings were performed twice for 1 hour, by using an

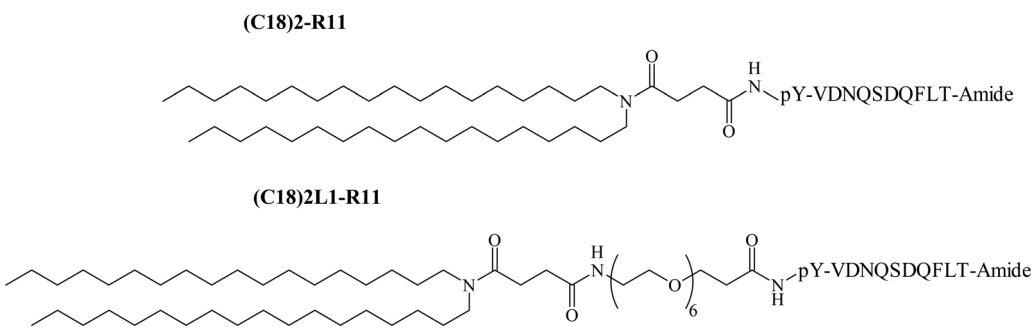

Fig. 1 Schematic representation of $(C18)_2$-R11 and $(C18)_2$-L1-R11 peptide amphiphiles (PAs). The peptide sequence is reported using the one-letter amino acid code.

excess of 4 equivalents for the single amino acid. To obtain $(C18)_2$-L1-R11 and $(C18)_2$-R11 peptide amphiphiles (PAs), the Fmoc-Ahoh-OH derivative and *N*,*N*-dioctadecylsuccinamic acid were coupled as previously described.[30] Peptides were fully deprotected and cleaved from the resin with TFA with 2.5% (v/v) water and 2.5% (v/v) TIS as scavengers, at room temperature. The R11 peptide was precipitated with ice-cold ethyl ether, while PAs were precipitated with water.[31]

2.4. Preparation of the solutions

All solutions were prepared by weight and simply dissolved in 0.10 M phosphate buffer (PBS) at pH 7.4. The pH-meter was calibrated with three standards at pH 4.00, pH 7.00 and pH 10.00. In most cases the samples to be measured were prepared from stock solutions. Concentrations of all solutions were determined by absorbance on a UV-Vis Jasco (Easton, MD) Model V-5505 spectrophotometer equipped with a Jasco ETC-505T Peltier temperature controller with a 1 cm quartz cuvette (Hellma) using a molar absorption coefficient (ε_{267}) of 652 M^{-1} cm^{-1} for the phosphorylated tyrosine (pY) residue.[32]

2.5. Fluorescence measurements

The values of critical micellar concentrations (CMC) of peptide amphiphiles $(C18)_2$R11 or $(C18)_2$-L1-R11 were obtained by fluorescence measurements. Fluorescence spectra were recorded at room temperature on a Jasco Model FP-750 spectrofluorophotometer in a 1.0 cm path length quartz cell. Equal excitation and emission bandwidths were used throughout the experiments, with a recording speed of 125 nm min^{-1} and automatic selection of the time constant. The CMC were measured by using 8-anilino-1-naphthalene sulfonic acid ammonium salt (ANS) as the fluorescent probe.[33] Small aliquots of 1×10^{-5} M peptide solution, dissolved in 0.1 M phosphate buffer at pH 7.4, were added to a fixed volume (1.00 mL) of fluorophore (1×10^{-5} M ANS) directly in the quartz cell. CMC values were determined by linear least-squares fitting of the fluorescence emission at 480 nm, upon excitation at 350 nm *versus* the amphiphile concentration.

2.6. DLS characterization

Dynamic light scattering measurements were carried out using a Zetasizer Nano ZS (Malvern Instruments, Westborough, MA) that employs a 173° backscatter detector. Other instrumental settings are measurement position (mm): 4.65; attenuator: 8; temperature 25 °C; cell: disposable sizing cuvette. DLS samples were prepared at a final concentration of 3×10^{-4} M and centrifuged at room temperature at 13 000 rpm for 5 min.

2.7. Monomolecular film experiments

Surface pressure–molecular area (π–A) isotherms were recorded for $(C18)_2$R11 and $(C18)_2$-L1-R11 using a KSV 5000 tensiometer and a Teflon trough (61.0 mm width × 345.0 mm length × 1.0 mm height) equipped with a mobile Teflon barrier and placed inside a thermostated chamber at 25 °C. Surface pressure was measured using a Wilhelmy plate (perimeter 3.94 cm) attached to an electromicrobalance connected to a microprocessor controlling the movements of the mobile barrier. For compression isotherms, the speed of the barrier was 10 mm min^{-1}. Cycles of compression–decompression isotherms were also performed at a speed of 10 mm min^{-1}, with hold times of 1 and 30 seconds after compression and decompression, respectively. Before each experiment, the trough and the mobile barrier were thoroughly cleaned with tap water, then gently brushed in the presence of distilled ethanol, before being washed again with tap water and finally rinsed with double-distilled water. Any residual surface active impurity was removed before each assay by sweeping and suction of the surface.

Before performing compression isotherms, the trough was filled with either 10 mM Tris buffer containing 100 mM NaCl, 21 mM $CaCl_2$ and 1 mM EDTA, or 0.1 M phosphate buffer, both prepared with double-distilled water and adjusted at pH 7.4. The peptide amphiphile monolayer was then formed by spreading a solution of $(C18)_2$R11 (58 μL) or $(C18)_2$-L1-R11 (66 μL) at 1 mg mL^{-1} in chloroform, using a Hamilton microsyringe. Ten minutes after spreading the peptide solution, the compression of the monolayer (in the gaseous state) was started and surface pressure recorded. For each pressure, the apparent molecular area of PA was deduced from the amounts of PA spread at the surface of the trough and the area covered by the film. All isotherm data herein presented could be repeated ($n = 3$) with a coefficient of variation not exceeding 5%.

2.8. CD measurements

Far-UV CD spectra were recorded from 190 to 260 nm on a Jasco J-810 spectropolarimeter equipped with a NesLab RTE111 thermal controller unit using a 1 mm quartz cell at 25 °C. Circular dichroism measurements were carried out on 0.1 M phosphate solutions containing peptide R11 or peptide amphiphile $(C18)_2$R11 or $(C18)_2$-L1-R11 at a concentration of 2×10^{-4} M at pH 7.4. Solutions of peptide were prepared in 0.1 M phosphate buffer at pH 7.4. Other experimental settings were: scan speed, 10 nm min^{-1}; sensitivity, 50 mdeg; time constant, 16 s; bandwidth, 1 nm. Each spectrum was obtained by averaging three scans, and by subtracting contributions from other species in solution.

2.9. NMR measurements

NMR samples of R11 and $(C18)_2$-L1-R11 were dissolved in 0.10 M sodium phosphate buffer at pH 7.4, at a concentration of $\sim 1 \times 10^{-3}$ M in a volume of 600 μL with 5% v/v D_2O (99.98% D, Armar Chemicals, Switzerland). Spectra of $(C18)_2$-R11 were recorded for two different samples at the concentrations of 1.40×10^{-3} M and 0.140×10^{-3} M respectively (in 600 μL of a 0.10 M sodium phosphate buffer at pH 7.4 with 5% v/v D_2O).

1D ^{1}H, 2D [^{1}H, ^{1}H] TOCSY (70 ms mixing time)[34] and 2D [^{1}H, ^{1}H] NOESY[35] experiments (mixing times: 50, 100, 150, 200 and 300 ms) were acquired at 298 K on a Varian Unity Inova 600 MHz spectrometer equipped with a cold-probe. 2D spectra were usually recorded with a number of scans ranging from 16 to 64, 128-256 FIDs in *t*1, 1024 or 2048 data points in *t*2. Water suppression was achieved with the DPFGSE (Double Pulsed Field Gradient Selective Echo) sequence.[36] The Varian software

VNMRJ 1.1D was implemented to process NMR spectra that were afterwards analyzed with the software NEASY[37] included in CARA (http://www.nmr.ch/).

Proton resonances were assigned with a standard procedure[38] based on comparison of 2D [^{1}H, ^{1}H] TOCSY[34] and 2D [^{1}H, ^{1}H] NOESY.[35] Chemical shifts were referenced to the water signal at 4.75 ppm.

3. Results and discussion

3.1. Peptide selection

The ability of a peptide to fold or not to fold is encoded in its amino acid sequence.[12] Usually the combination of low mean hydrophobicity and high net charge residues is an important prerequisite for the absence of compact structure. A peptide sequence of 20 amino acids in length, enriched in disorder-promoting amino acids, was conceived and its predicted disorder was analyzed and confirmed using the MeDor metaserver.[17] After prediction, the initial sequence was shortened so as to get a more drug-like molecule that could be easily modified from the synthetic point of view and that can enable future design of peptide libraries. Additionally, a Phe and a Leu residue were added before the C-terminal Thr amino acid, and a phosphotyrosine (pY) was added at the N-terminus. The rationale for adding these bulky residues was to introduce two possible interaction-prone sites, as hydrophobic and in particular aromatic residues are frequently used by IDPs to establish contacts with their partners.[39] In order to promote the formation of stable supramolecular aggregates in water, two lipophilic derivatives ($(C18)_2$-R11 and $(C18)_2$-L1-R11) were synthetized (Fig. 1). Both peptide amphiphiles (PAs) were obtained by introducing two alkyl chains of eighteen carbon atoms at the N-terminus. Moreover, $(C18)_2$-L1-R11 contains a unit of 21-amino-4,7,10,13,16,19-hexaoxaheneicosanoic acid (AhOh) between the peptide sequence and the hydrophobic double-tail with respect to $(C18)_2$-R11. This ethoxylic moiety used as a spacer/linker confers to the peptide an increased hydrophilicity and accessibility without modifying the final charge of the molecule. Moreover the ethoxylic-based spacer could be useful for future applications, being able to hide the supramolecular aggregates to the reticulo-endothelial system.[40]

3.2. Peptide synthesis and aggregates formulation

The R11 peptide and its lipophilic derivatives ($(C18)_2$-R11 and $(C18)_2$-L1-R11) were synthesized by solid-phase methods using Rink-amide MBHA resin as a polymeric support and the Fmoc/*t*Bu chemistry according to standard SPPS protocols.[41] Both lipophilic derivatives were obtained by coupling *N*,*N*-dioctadecylsuccinamic acid at the free N-terminus. $(C18)_2$-L1-R11 contains a unit of hexaoxaheneicosanoic acid between the R11 peptide and the alkyl chains with respect to $(C18)_2$-R11. The products, purified by preparative reverse-phase high-performance liquid chromatography (RP-HPLC), were isolated in good yields and their purity was assessed using analytical HPLC and electrospray ionization mass spectrometry (ESI-MS). HPLC purification of the R11 peptide was performed in high yields by a C18 column, according to standard procedures. Conversely, purification of the lipophilic peptide derivatives required the use of a C4 column owing to the presence of the two long alkyl chains. Self-assembling supramolecular aggregates were formed by dissolving the lipophilic derivatives in 0.10 M phosphate buffer at pH 7.4.

3.3. Structural characterization

The aggregation properties of the lipophilic peptides were investigated by fluorescence spectroscopy and dynamic light scattering (DLS). Apparent critical micellar concentration (CMC) values were determined by a fluorescence-based method using ANS as a probe. The fluorescence intensity at 480 nm, corresponding to the maximum of the spectrum, as a function of the PA concentration is reported in Fig. 2, where apparent CMC values can be visualized by the graphical break point. As reported in Table 1, the apparent CMC values of $(C18)_2$-L1-R11 and $(C18)_2$-R11 (5×10^{-5} and 6×10^{-5} M, respectively) are quite similar, thus indicating that the presence of an ethoxilic linker between the peptide and the alkyl tails does not influence the formation of aggregates capable of sequestering the ANS. These values are in good agreement with those previously reported for double-tailed PAs.[42]

The mean diameter of the aggregates was assessed by dynamic light scattering. Measurements were performed at $\theta = 173^\circ$ on self-assembled PAs at a concentration of 2×10^{-4} M in 0.1 M phosphate buffer at pH 7.4. The $(C18)_2$-R11 peptide shows a monomodal distribution, which could be attributed to aggregated structures with apparent translational diffusion coefficients D_{slow} (see Fig. 3A and Table 1). Instead, the

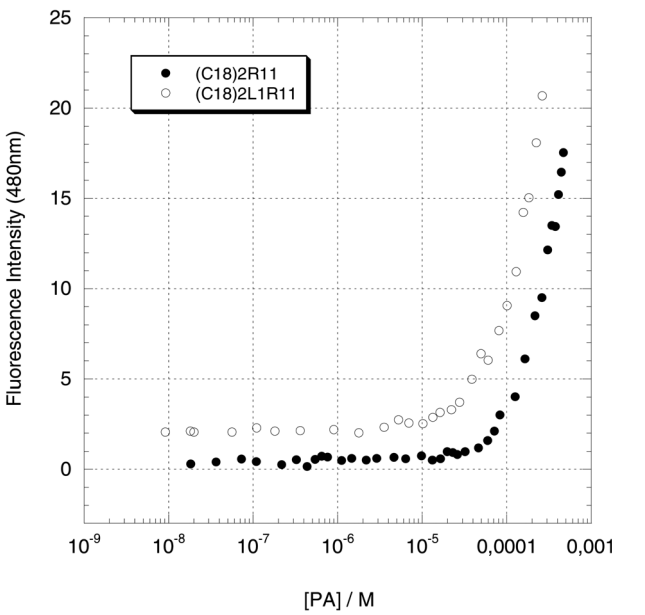

Fig. 2 Fluorescence intensity of the ANS fluorophore at 480 nm as a function of PAs concentration; data are multiplied by a scale factor for a better comparison. CMC values (5.0×10^{-5} and 6.0×10^{-5} M) are established from graphical break points.

Table 1 Critical micellar concentration (CMC) values determined by fluorescence and diffusion coefficients (D) and hydrodynamic radii (R_H) obtained from dynamic light scattering measurements for the systems studied. The terms fast and slow refer to smaller and larger aggregates, respectively

Systems	CMC (mol kg^{-1})	$D_{fast} \times 10^{-11}$ (m^2 s^{-1})	Mean diameter (nm)	$D_{slow} \times 10^{-12}$ (m^2 s^{-1})	Mean diameter (nm)
$(C18)_2$R11	6.0×10^{-5}	—	—	2.26 ± 0.85	185.663 ± 70.16
$(C18)_2$-L1-R11	5.0×10^{-5}	3.11 ± 0.79	15.76 ± 4.00	2.02 ± 0.74	243.02 ± 89.28

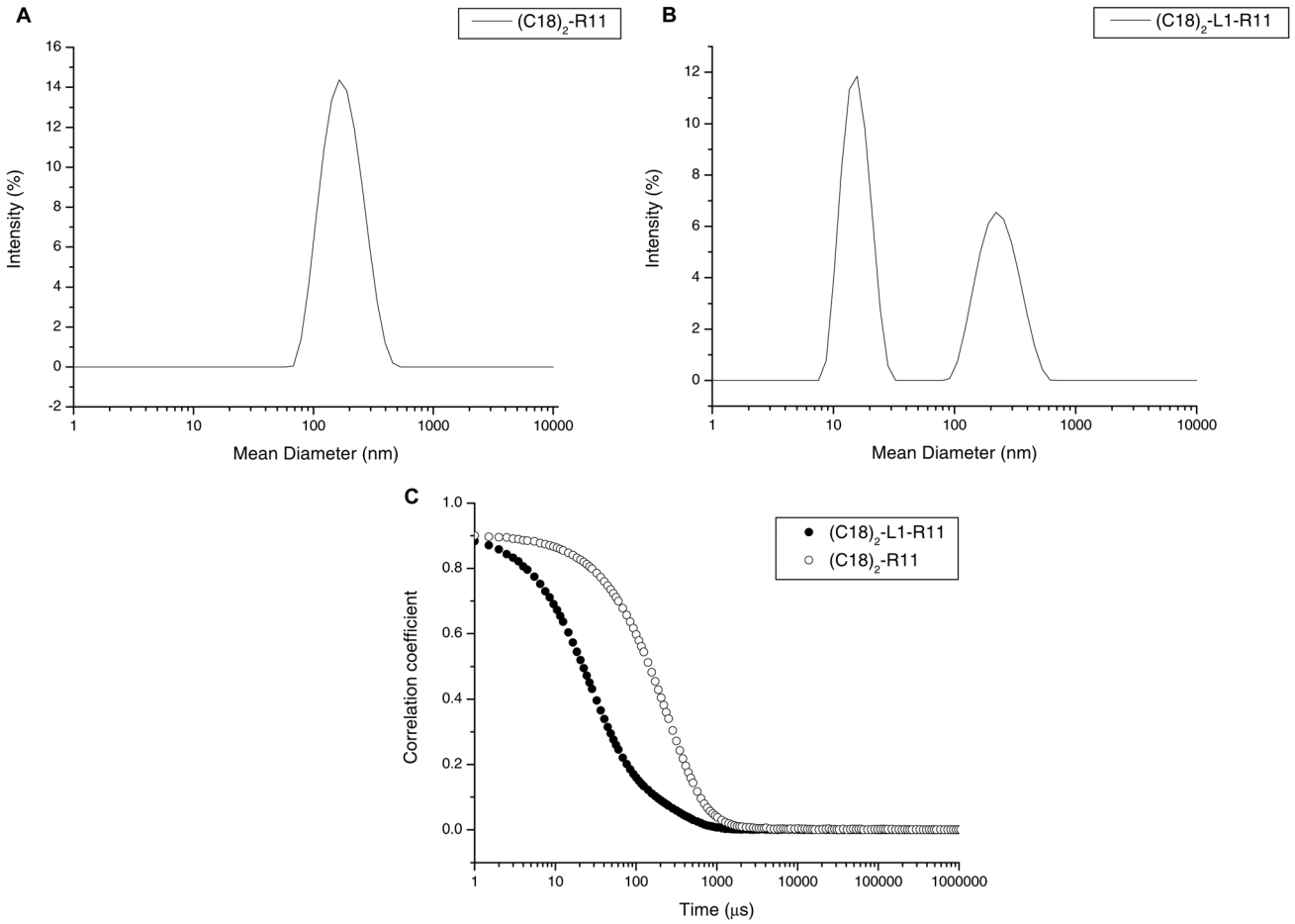

Fig. 3 DLS spectra of $(C18)_2$-R11 (A) and $(C18)_2$-L1-R11 (B) peptide amphiphiles at a concentration of 1×10^{-4} M; (C) intensity correlation functions at θ 173° for $(C18)_2$-R11 and $(C18)_2$-L1-R11 solutions at 1×10^{-4} M.

distribution of the $(C18)_2$-L1-R11 peptide is bimodal and dominated by the fast mode (Fig. 3B). For a better comparison between the two PAs, the correlation functions are reported in Fig. 3C. The Stokes–Einstein eqn (1) is used to evaluate the hydrodynamic radius, R_H, at infinite dilution

$$R_H = \frac{K_B T}{6\pi\eta D_0} \quad (1)$$

where D_0 is the translational diffusion coefficient at infinite dilution, K_B is the Boltzmann constant, T is the absolute temperature, and η is the solvent viscosity. Due to the high solution dilution ($C = 1 \times 10^{-4}$ M) of the systems under study, we have approximately $D \sim D_0$, and eqn (1) can be reasonably used to estimate the hydrodynamic radius of the aggregates. The mean diameter values obtained for slow and fast modes (Table 1) are compatible with the formation of large supramolecular aggregates (mean diameter of around 184–242 nm) for both PAs, as well as with small aggregates in the case of $(C18)_2$-L1-R11 (mean diameter of around 16 nm). The size of the large molecular aggregates would support the formation of small unilamellar vesicles/liposomes (SUV, 100 nm range) as observed with phospholipids. Small molecular aggregates would rather correspond to the formation of micelles. Both micelles and liposomes seem therefore to coexist in the case of $(C18)_2$-L1-R11. Based on the DLS results, the CMC determination by fluorescence spectroscopy has to be taken with caution since ANS can also be incorporated in vesicles.

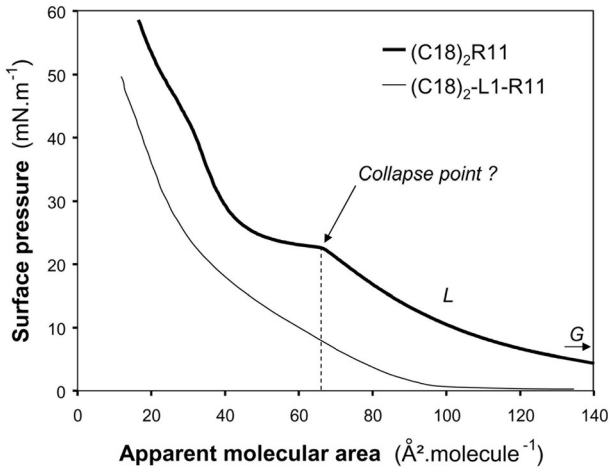

Fig. 4 Surface pressure–area (π–A) isotherms obtained with the $(C18)_2$-R11 and $(C18)_2$-L-R11 peptide amphiphiles spread at the air–water (Tris buffer) interface at 25 °C. The buffer contained 10 mM Tris, 100 mM NaCl, 21 mM $CaCl_2$, 1 mM EDTA and the pH was adjusted to 7.4. The various phases are indicated by letters (gaseous state, G; liquid state, L) and the putative collapse point of $(C18)_2$-R11 is indicated by an arrow.

3.4. Interfacial properties of PAs

Langmuir films were formed at the air–water interface by spreading known amounts of $(C18)_2$-R11 or $(C18)_2$-L1-R11 and variations in surface pressure were recorded upon compression of the film. The surface pressure–area (π–A) isotherm of the $(C18)_2$-R11 PA spread on Tris buffer pH 7.4 showed an intermediate plateau with the surface pressure remaining constant while the molecular area decreased, suggesting a collapse of the PA monolayer (Fig. 4). The collapse parameters (molecular area, A_{coll}; surface pressure, Π_{coll}) were determined at the point of highest compressibility (C = 0.555 m mN^{-1}) estimated from the compression isotherm[43,44] and were found to be A_{coll} = 64.5 $Å^2$ and Π_{coll} = 22.8 mN m^{-1}. The molecular area at collapse fits with previous data obtained with phospholipids bearing two C18 chains.[44] For instance, dioleoyl-phosphatidylcholine shows an A_{coll} of 62.9 $Å^2$ (Π_{coll} = 43.5 mN m^{-1}) at pH 5.5 and 59.6 $Å^2$ (Π_{coll} = 48 mN m^{-1}) at pH 8, while dioleoyl-phosphatidylinositol has an A_{coll} of 66.2 $Å^2$ (Π_{coll} = 42 mN m^{-1}) at pH 5.5 and 62.9 $Å^2$ (Π_{coll} = 46.5 mN m^{-1}) at pH 8.[44] Collapse however occurred at lower surface pressures in the case of $(C18)_2$-R11 PA and a further increase in surface pressure upon compression was observed after the plateau (Fig. 4). This profile suggests that aggregates of $(C18)_2$-R11 PA are formed above the collapse point and are further expelled from the interface when the interfacial area is decreased. As shown in Fig. 4, the apparent molecular area of $(C18)_2$-L1-R11 was lower under similar conditions and no collapse point was observed. The formation and solubilization of aggregates seem to be more important in that case, as suggested by the higher compressibility and thus the "more liquid" nature of the PA film. Micelle formation is probably the reason for the leakage of $(C18)_2$-L1-R11 molecules from the monolayer during compression.

Similar experiments were performed with 0.1 M phosphate buffer, pH 7.4 in order to reproduce the buffer conditions used for DLS and NMR experiments. The apparent molecular area of $(C18)_2$-R11 was still higher than that of $(C18)_2$-L1-R11 (Fig. 5) but the surface pressure–area isotherm (Fig. 5A) had a distinct pattern with respect to that obtained with Tris buffer (Fig. 4). No collapse plateau was observed for $(C18)_2$-R11. The apparent molecular areas of $(C18)_2$-R11 at 24 and 30 mN m^{-1} (88.5 to 74 $Å^2$, respectively) were higher than those recorded with Tris buffer (Fig. 4). These findings suggest that part of the peptide moiety could also be inserted in the monolayer at the air–water interface. The surface pressure–area isotherms recorded upon successive cycles of compression–decompression of the $(C18)_2$-R11 monolayer showed a large and reproducible hysteresis, indicating that part of $(C18)_2$-R11 transferred to the water subphase upon compression underwent a reversible process with slow kinetics. A hysteresis, though less marked, was also observed with $(C18)_2$-L1-R11 (Fig. 5B).

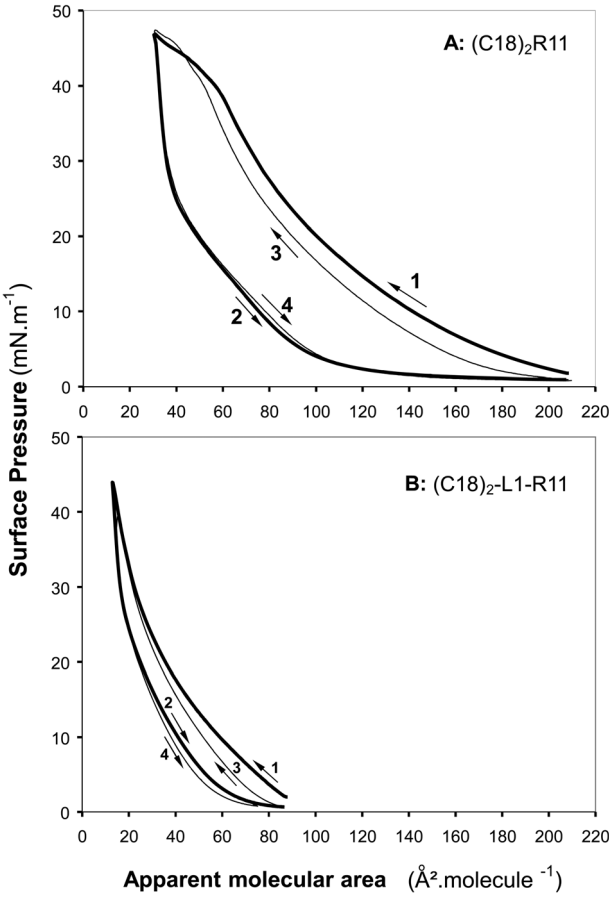

Fig. 5 Cycles of compression–decompression of $(C18)_2$-R11 (A) and $(C18)_2$-L-R11 (B) monomolecular films at the air–water (phosphate buffer) interface at 25 °C. The pH of the 100 mM phosphate buffer was adjusted to 7.4. The numbers 1 (compression)–2 (decompression) and 3 (compression)–4 (decompression) correspond to the first and second cycles, respectively.

3.5. CD measurements

Circular Dichroism (CD) spectroscopy is broadly used to diagnose the presence of secondary structure features in peptides or proteins. In the last years, CD has been currently employed to

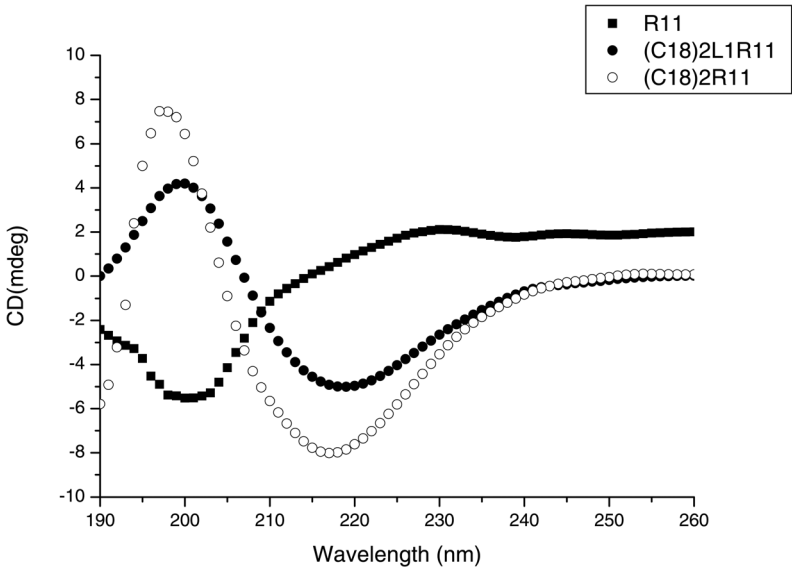

Fig. 6 Far-UV CD spectra of the R11 peptide and of the $(C18)_2$-R11 and $(C18)_2$-L1-R11 peptide amphiphiles at pH 7.4. The concentration of both PAs is 2.0×10^{-4} M, well above the CMC so as to ensure the presence of aggregates in solution.

characterize the morphology of aggregates obtained by PAs as a function of pH.[45] Fig. 6 shows a comparison of the CD spectra of the R11 peptide and of the PAs at concentrations above their apparent CMC values (2×10^{-4} M). The CD spectrum of the R11 phosphopeptide in PBS presents a negative band centred at 201 nm, typical of unstructured peptides, thereby confirming MeDor predictions. In contrast, the CD spectra of PAs show a large minimum at 218 nm, and a maximum at 198 nm, typical of the presence of β-strands. Since only the peptide moiety contributes to the signal, these results suggest that the presence of the alkyl chains induces a disorder to order transition, and in particular an enrichment in the β content.

3.6. NMR studies

NMR studies of different PAs, conducted in aqueous buffer and in the presence of amphiphilic molecules, such as sodiumdodecylsulphate (SDS, anionic) and *n*-dodecyl phosphatidylcholine (DPC, zwitterionic), have previously been reported.[46–48] Interestingly, Behanna *et al.*[46] studied nanofibers generated by mixing together different PAs containing alkyl chains linked at either their N-terminal or C-terminal peptide side, and used 2D [^{1}H, ^{1}H] NOESY experiments[35] to prove intermolecular contacts between different PA units. Moreover, Fields[48] demonstrated by CD and NMR techniques that the self-assembly of PAs could favor the formation of protein-like structural topologies. In the current work, we used 1D and 2D proton NMR spectroscopy to investigate the conformational properties in solution of the R11, $(C18)_2$-L1-R11 and $(C18)_2$-R11 peptides. We first analyzed the R11 peptide in aqueous buffer (0.10 M sodium phosphate pH 7.4) at a concentration of $\sim 1 \times 10^{-3}$ M. Under these experimental conditions, R11 is highly flexible and lacks ordered secondary structure elements as indicated by the nearly complete absence of the signal in the 2D [^{1}H, ^{1}H] NOESY experiment[35] (data not shown). In the case of $(C18)_2$-L1-R11, we carried out a detailed NMR analysis. High quality NMR spectra, containing sharp signals, could in fact be recorded in phosphate buffer. We could get resonance assignments for most of the C18 alkyl tails, linker and peptide protons (Table S1, ESI‡). Analysis of the 2D [^{1}H, ^{1}H] NOESY spectrum revealed NOEs between the CH_2 groups from the C18 alkyl chains and peptide protons (Fig. 7, lower panel). Correlations between these methylene groups at 1.17 ppm (Table S1, ESI‡) and aromatic protons of Phe and pTyr could be unambiguously assigned. Strong NOEs arising from correlations between peptide aromatic protons and CH_2 protons of the spacer, which resonate at 3.55, 3.51, 2.55 and 2.42 ppm, could be identified as well (Table S1, ESI‡, and Fig. 7, lower panel). As for the peptide portion of the molecule, sequential NOEs characteristic of extended conformations could be detected (Fig. 7, upper panel). According to DLS measurements, the sharpness of the NMR signals let us speculate that, under the experimental conditions used to run the NMR experiments, $(C18)_2$-L1-R11 forms small supramolecular aggregates. Besides, our data indicate that the peptide region does indeed interact with both the C18 chains and the linker. This scenario is probably favored by the ethoxylic spacer that interposed between the peptide and the alkyl chain, confers to $(C18)_2$-L1-R11 a certain degree of flexibility in solution. This flexibility could promote the insertion of the peptide into the hydrophobic core of $(C18)_2$-L1-R11 aggregates and destabilize the supramolecular packing with a significant decrease in the aggregation number. This could explain why both micellar and liposome-like aggregates are observed with $(C18)_2$-L1-R11 using DLS.

Afterwards, we analyzed by NMR the $(C18)_2$-R11 peptide (1.4×10^{-3} M concentration). In this case, formation of aggregates, produced by self-association, is evident in the 2D [^{1}H, ^{1}H] TOCSY[34] and NOESY[35] experiments whose sensitivity is

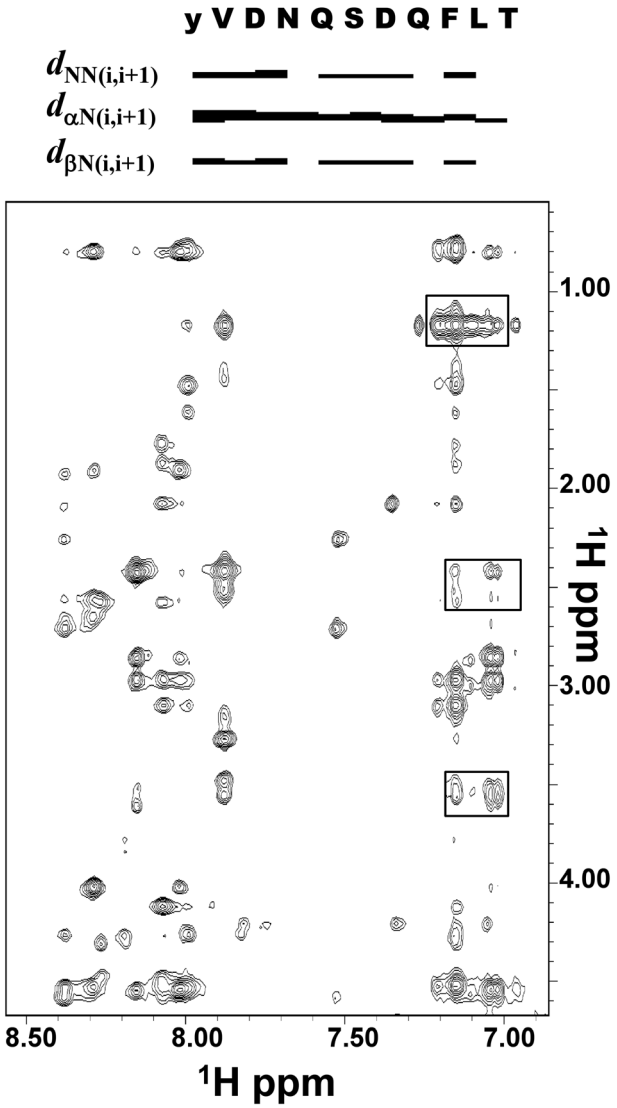

Fig. 7 (Upper panel) Pattern of sequential NOEs for the $(C18)_2$-L1-R11 peptide. The one letter amino acid code is used for the different residues, *y* stands for phosphotyrosine; $d_{AB}(i, i + 1)$ represents a NOE contact between protons H_A and H_B of the *i* and *i* + 1 amino acids respectively. The thickness of the bars is proportional to the corresponding peak intensity. The graph has been generated with Cyana 2.1.[49] (Lower panel) Expansion of the 2D [^{1}H, ^{1}H] NOESY 200 spectrum of $(C18)_2$-L1-R11. In the reported region, correlations belonging to H_N and aromatic protons can be observed; the rectangles highlight cross-peaks between aromatic protons of Phe and pTyr and CH_2 protons from the alkyl terminal chains and linker.

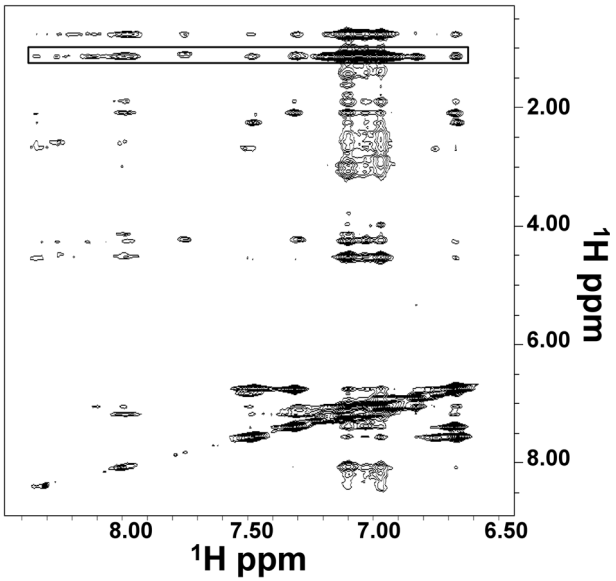

Fig. 8 2D [^{1}H, ^{1}H] NOESY 200 spectrum of the $(C18)_2$-R11 peptide (at 1.40 × 10^{-3} M concentration in 0.10 M phosphate buffer pH 7.4). An expansion containing peaks arising from H_N and aromatic protons is shown. The rectangle encompasses cross-peaks between CH_2 protons of the alkyl chains and peptide moieties.

reduced by line broadening (Fig. 8). Detailed NMR characterization for $(C18)_2$-R11 was not achievable. However, as shown in Fig. 8, NOEs between the CH_2 protons of the C18 alkyl chains and either peptide H_N or aromatic protons appear rather clear and strong (Fig. 8). Line broadening also affected NMR spectra recorded on a $(C18)_2$-R11 sample after a ten-fold dilution (final concentration equal to 0.140 × 10^{-3} M), thus confirming the high tendency of this PA to self-associate. We can speculate, in agreement with dynamic light scattering data, that larger aggregates are formed by $(C18)_2$-R11 with respect to $(C18)_2$-L1-R11 and that at least a few peptide moieties lie in these supramolecular systems in a way that enables them to contact the C18 alkyl chains.

4. Conclusions

PAs have already deserved various investigations but this is the first time an intrinsically disordered peptide is used as a polar head connected to alkyl chains. Overall, the physical methods used in this study allowed us to describe the self-assembly of $(C18)_2$-R11 and $(C18)_2$-L1-R11 in supramolecular aggregates compatible with unilamellar vesicles and micelles, respectively (Fig. 9). The characterization of this new class of PAs by far-UV CD spectroscopy showed that the high flexibility of the free R11 peptide is reduced in both lipophilic peptides and suggests that these compounds can undergo some disorder-to-order transition upon their self-assembly in supramolecular aggregates. The study of the interfacial behavior of these new PAs by the Langmuir film technique showed that they are endowed with features typical of surfactant molecules. These new amphiphiles have mainly a fundamental interest at this point, but their supramolecular aggregates presenting an ordered core and a ''disordered'' surface might later be used as scaffolds for developing applications in chemistry and medicine. Indeed, the ability of the alkyl chains to trigger a gain of structure within the disordered peptide could be used to modulate PA molecules able to form more sophisticated architectures. These new PAs could be engineered for applications in the encapsulation of living cells as well as in biomedical engineering and in biocompatible materials. The design of supramolecular systems, generated by joining together a disordered peptide and a lipophilic moiety, could drive the disordered peptide to fold

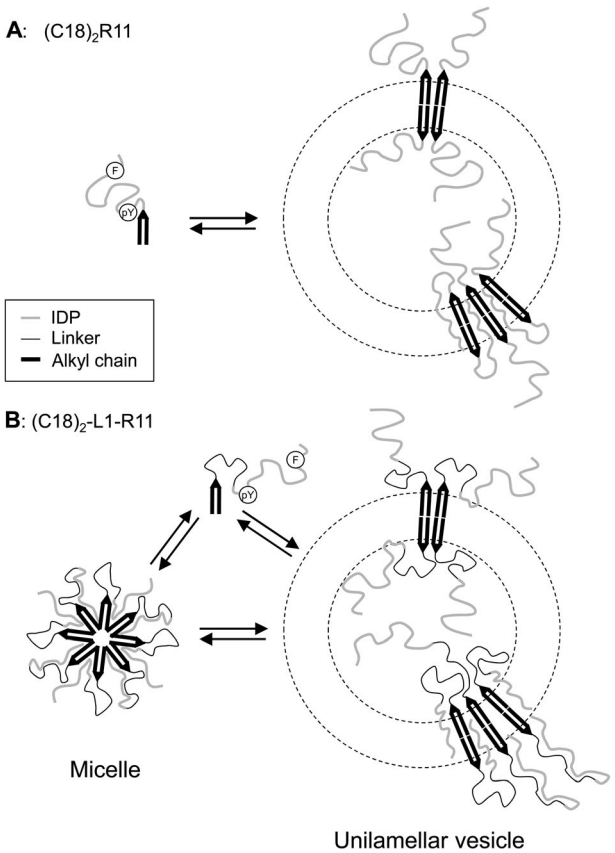

Fig. 9 Schematic representation of the molecular aggregates formed in water by $(C18)_2$-R11 (A) and $(C18)_2$-L-R11 (B) PAs. This representation takes into account the experimental data obtained by DLS (size and type of aggregates), NMR (molecular interactions of the peptide moiety with the alkyl chain and linker methylene groups), and monolayer experiments (interfacial properties). The position of the aromatic residues (pY and F) on the peptide chain is indicated only in the PA monomers, but the drawing of the $(C18)_2$-L1-R11 micelle takes into account the interaction between these residues and the alkyl chain and linker methylene groups (NMR data) depending on the PA conformation. These interactions were also taken into account when drawing some of the PA conformations in unilamellar vesicles.

into a stable structure. This structural modification could be a promising route to develop a new class of bio-molecules for processes in which a specific conformational rearrangement is required.

Abbreviations

AhOh	21-Amino-4,7,10,13,16,19-hexaoxaheneicosanoic acid
ANS	8-Anilinonaphthalene-1-sulfonate
CMC	Critical micellar concentration
CD	Circular dichroism
DIPEA	*N,N*-Diisopropylethylamine
DLS	Dynamic light scattering
DMF	*N,N*-Dimethylformamide
DPC	*n*-Dodecyl phosphatidylcholine
EDTA	Ethylenediaminetetraacetic acid
Fmoc	9-Fluorenylmethoxycarbonyl
HOBt	1-Hydroxybenzotriazole
NOESY	Nuclear overhauser enhancement spectroscopy
PA	Peptide amphiphile
RP-HPLC	Reverse-phase high-pressure liquid chromatography
pY	Phosphotyrosine
PyBop	Benzotriazol-1-yl-oxy-tris-pyrrolidino-phosphonium
SDS	Sodiumdodecylsulphate
TFA	Trifluoroacetic acid
TIS	Triisopropylsylane
TOCSY	Total correlation spectroscopy

Acknowledgements

The authors thank Mr Leopoldo Zona for NMR experimental assistance and Mr Luca De Luca for his informatics assistance in the working of all equipment.

References

1 G. Wider, K. H. Lee and K. Wuthrich, *J. Mol. Biol.*, 1982, **155**, 367–388.
2 L. Zetta, P. J. Hore and R. Kaptein, *Eur. J. Biochem.*, 1983, **134**, 371–376.
3 F. Naider, L. A. Jelicks, J. M. Becker and M. S. Broido, *Biopolymers*, 1989, **28**, 487–497.
4 L. R. Brown, W. Braun, A. Kumar and K. Wuthrich, *Biophys. J.*, 1982, **37**, 319.
5 J. K. Lakey, D. Baty and F. Pattus, *J. Mol. Biol.*, 1991, **218**, 639–653.
6 V. Bernier, M. Lagacé, D. G. Bichet and M. Bouvier, *Trends Endocrinol. Metab.*, 2004, **15**, 222–228.
7 A. Ulloa-Aguirre, J. A. Janovick, S. P. Brothers and P. M. Conn, *Traffic*, 2004, **5**, 821–837.
8 C. M. Dobson, *Trends Biochem. Sci.*, 1999, **24**, 329–332.
9 P. Bernardo, C. W. Bertoncini, C. Greisinger, M. Zweckstetter and M. Blackledge, *J. Am. Chem. Soc.*, 2005, **127**, 17968–17969.
10 K. Toriumi, Y. Oma, Y. Kino, E. Futai, N. Sasagawa and S. Ishiura, *J. Neurosci. Res.*, 2008, **86**, 1529–1537.
11 M. D. Mukrasch, P. Martkiwick, J. Bierat, M. von Bergen, P. Bernado, C. Greisinger, E. Mandelkow, M. Zweckstetter and M. Blackledge, *J. Am. Chem. Soc.*, 2007, **129**, 5235–5243.
12 V. Uversky and A. K. Dunker, *Biochim. Biophys. Acta*, 2010, **1804**, 1231–1264.
13 R. Schweitzer-Stenner, *Mol. BioSyst.*, 2012, **8**, 122–133.
14 V. N. Uversky, *Int. J. Biochem. Cell Biol.*, 2011, **43**, 1090–1103.
15 S. Banta, Z. Megeed, M. Casali, K. Rege and M. L. Yarmush, *J. Nanosci. Nanotechnol.*, 2007, **7**, 387–401.
16 K. Chockalingam, M. Blenner and S. Banta, *Protein Eng., Des. Sel.*, 2007, **20**, 155–161.
17 P. Lieutaud, B. Canard and S. Longhi, *BMC Genomics*, 2008, **9**(suppl. 2), S25.
18 A. Trent, R. Marullo, B. Lin, M. Black and M. Tirrell, *Soft Matter*, 2011, **7**, 9572–9582.
19 I. W. Hamley, *Soft Matter*, 2011, **7**, 4122–4138.
20 F. Versluis, H. R. Marsden and A. Kros, *Chem. Soc. Rev.*, 2010, **39**, 3434–3444.
21 X. Zhao, F. Pan, H. Xu, M. Yaseen, H. Shan, C. A. Hanser, S. Zhang and J. R. Lu, *Chem. Soc. Rev.*, 2010, **39**, 3480–3498.

22 H. Cui, M. J. Webber and S. I. Stupp, *Biopolymers*, 2010, **94**, 1–18.
23 S. E. Paramonov, H.-W. Jun and J. D. Hartgerink, *J. Am. Chem. Soc.*, 2006, **128**, 7291–7298.
24 R. Pajewski, R. Ferdani, J. Pajewska, L. Djedovic, P. H. Schlesinger and G. W. Gokel, *Org. Biomol. Chem.*, 2005, **3**, 619–625.
25 A. Accardo, D. Tesauro, P. Roscigno, E. Gianolio, L. Paduano, G. D'errico, C. Pedone and G. Morelli, *J. Am. Chem. Soc.*, 2004, **126**, 3097–3107.
26 A. Accardo, A. Morisco, P. Palladino, R. Palumbo, D. Tesauro and G. Morelli, *Mol. BioSyst.*, 2011, **7**, 862–870.
27 F. Bernal, A. F. Tyler, S. J. Korsmeyer, L. D. Walensky and G. L. J. Verdine, *J. Am. Chem. Soc.*, 2007, **129**, 2456–2457.
28 D. Missirlis, D. V. Krogstad and M. Tirrell, *Mol. Pharmaceutics*, 2010, **7**, 2173–2184.
29 L. Schmitt and C. Dietrich, *J. Am. Chem. Soc.*, 1994, **116**, 8485–8491.
30 A. Accardo, R. Mansi, A. Morisco, G. Mangiapia, L. Paduano, D. Tesauro, A. Radulescu, M. Aurilio, L. Aloj, C. Arra and G. Morelli, *Mol. BioSyst.*, 2010, **6**, 878–887.
31 A. Morisco, A. Accardo, E. Gianolio, D. Tesauro, E. Benedetti and G. Morelli, *J. Pept. Sci.*, 2009, **15**, 242–250.
32 A. R. Grucza, J. M. Bradshaw, V. Mitaxov and G. Waksman, *Biochemistry*, 2000, **39**, 10072–10081.
33 A. Accardo, D. Tesauro, G. Mangiapia, C. Pedone and G. Morelli, *Biopolymers*, 2007, **88**, 115–121.
34 C. Griesinger, G. Otting, K. Wüthrich and R. R. Ernst, *J. Am. Chem. Soc.*, 1988, **110**, 7870–7872.
35 A. Kumar, R. R. Ernst and K. Wuthrich, *Biochem. Biophys. Res. Commun.*, 1980, **95**, 1–6.
36 C. Dalvit, *J. Biomol. NMR*, 1998, **11**, 437–444.
37 C. Bartels, T. Xia, M. Billeter, P. Günthert and K. Wüthrich, *J. Biomol. NMR*, 1995, **6**, 1–10.
38 K. Wüthrich, *NMR of proteins, nucleic acids*, John Wiley & Sons, New York, 1986.
39 B. Mészáros, P. Tompa, I. Simon and Z. Dosztányi, *J. Mol. Biol.*, 2007, **372**, 549–561.
40 V. P. Torchilin, V. G. Omelyanenko, M. I. Papisov, A. J. Bogdano, V. S. Trubetskoy, J. N. Herron and C. A. Gentry, *Biochim. Biophys. Acta*, 1994, **119**, 11–20.
41 W. C. Chang and P. D. White, *Fmoc Solid Phase Peptide Synthesis*, Oxford Univ Press, 2000.
42 M. Vaccaro, G. Mangiapia, L. Paduano, E. Gianolio, A. Accardo, D. Tesauro and G. Morelli, *ChemPhysChem*, 2007, **8**, 2526–2538.
43 J. Rubio-Magnieto, S. V. Luis, M. Orlof, B. Korchowiec, G. Sautrey and E. Rogalska, *Colloids Surf., B*, 2013, **102**, 659–666.
44 M. Record, S. Amara, C. Subra, G. Jiang, G. D. Prestwich, F. Ferrato and F. Carrière, *Biochim. Biophys. Acta, Mol. Cell Biol. Lipids*, 2011, **1811**, 419–430.
45 A. Ghosh, M. Haverick, K. Stump, X. Yang, M. F. Tweedle and J. E. Goldberger, *J. Am. Chem. Soc.*, 2012, **134**, 3647–3650.
46 H. A. Behanna, J. J. J. M. Donners, A. C. Gordon and S. I. Stupp, *J. Am. Chem. Soc.*, 2005, **127**, 1193–1200.
47 N. A. Lockwood, J. R. Haseman, M. V. Tirrell and K. H. Mayo, *Biochem. J.*, 2004, **378**, 93–103.
48 G. B. Fields, *Bioorg. Med. Chem.*, 1999, **7**, 75–81.
49 T. Herrmann, P. Güntert and K. Wüthrich, *J. Mol. Biol.*, 2002, **319**, 209–227.

